Author Queries

AQ1 Details of Cargill Klimchuk 1997 and Paschmann et al 1979 are not found in the referance list please provide.
AQ2 Give a or b for Hesse et al. 2011.
AQ3 Sub zero meant?
AQ4 Note that Eqs have been renumbered.
AQ5 As meant?
AQ6 Harris, 1962 is not provided in the reference list.
AQ7 Not cited in text.
AQ8 Volume meant? give page(s).

15

Magnetic Reconnection in Different Environments: Similarities and Differences

Michael Hesse,[1] Nicolas Aunai,[1] Masha Kuznetsova,[1] Seiji Zenitani,[2] and Joachim Birn[2,3]

15.1. INTRODUCTION

Magnetic reconnection is broadly recognized as a key plasma transport and energy conversion process in space plasmas. Ranging from solar activity [e.g., *Cargill and Klimchuk*, 1997; *Antiochos et al.*, 1999] through interplanetary space [e.g., *Gosling et al.*, 1995, 2005] to the boundaries [e.g., *Paschmann et al.*, 1979; *Sonnerup et al.*, 1981] and interiors of planetary magnetospheres [e.g., Hones, 1977], magnetic reconnection facilitates highly time dependent, eruptive behavior and it transports mass, momentum, and energy into regions featuring otherwise nearly impenetrable boundary layers.

A key feature of magnetic reconnection is that it primarily converts magnetic energy in the two inflow regions into internal and kinetic energy. The efficacy of this energy conversion process depends strongly on plasma parameters in the two inflow regions [e.g., *Aunai et al.* 2011]. For example, high plasma $\beta = 2\mu_0 p/B^2$ [*Swisdak et al.*, 2003] or low Alfvén speed [*Hesse et al.*, 1996] in the inflow slows down the reconnection process.

In Earth's magnetosphere, magnetic reconnection operates both at the magnetopause, the boundary between solar-wind-dominated plasma and the region dominated by Earth's magnetic field, and on the nightside, within Earth's magnetotail. In the former situation, reconnection merges magnetic fields and plasmas of solar origin on one side with magnetospheric magnetic field and plasma on the other in a usually very asymmetric geometry [e.g., *Mozer et al* 2008]. Furthermore, reconnecting magnetic fields are typically not coplanar, implying, in the reconnection plane, the existence of an out-of-plane magnetic field. On the nightside, however, reconnection is believed to involve considerably more symmetric environments, with usually relatively small guide magnetic fields. It is expected that similar situations prevail at the other magnetized planets. Given the varied nature of the environments magnetic reconnection operates in, it is therefore of great interest to understand how reconnection adjusts to plasma parameters in both inflow regions.

Owing to its importance, reconnection has therefore been studied by means of spacecraft observations [e.g., *Eastwood et al.*, 2007, 2010; *Paschmann*, 2008], by analytic theory [*Cassak and Shay*, 2007; *Birn et al.*, 2011; *Hesse et al.*, 2011], and by numerical modeling. Recent work has indicated that reconnection changes substantially if the inflow sides are unequal [*Swisdak et al.*, 2003; *Mozer and Pritchett*, 2011; *Hesse et al.*, 2013] or if a guide magnetic field is being introduced [e.g., *Hesse et al.*, 2011]. Kinetic, hybrid, and Hall-MHD simulations consistently exhibit a reconnection rate much larger than typical Sweet-Parker rates [*Birn et al.*, 2001]; however, recent evidence suggests that island formation may impact reconnection rates in kinetic models [*Daughton et al.*, 2006, 2009, *Karimabadi et al.*, 2007], and it may play a critical role in enabling fast reconnection even in MHD systems [*Huang and Bhattacharjee*, 2013].

This chapter therefore addresses two important aspects of magnetic reconnection: time-dependent rates affected by island formation and the preferred direction of the

[1] *Heliophysics Science Division, NASA Goddard Space Flight Center, Greenbett, Maryland*
[2] *National Astronomical Observatory of Japan, Tokyo, Japan*
[3] *Space Science Institute, Boulder, Colorado*

Magnetotails in the Solar System, Geophysical Monograph 207. First Edition.
Edited by Andreas Keiling, Caitríona M. Jackman, and Peter A. Delamere.

reconnection line if merging magnetic field components are not antiparallel. The former presents new results, whereas the latter will summarize recent findings [*Hesse et al.*, 2013]. The two aspects of the analysis will be prefaced by a basic discussion of the impact magnetic reconnection has on energy transport across topological boundaries.

15.2. ENERGY TRANSPORT

While it is widely known that magnetic reconnection facilitates mass, momentum, and energy transport in plasmas, it is illustrative to consider an analytical approach to describing the efficacy of reconnection as a transport mechanism. For simplicity, we consider a simple, two-dimensional geometry, where an X-shaped reconnection region forms the intersection of two separatrices. The geometry is depicted in Figure 15.1.

Here, V denotes the volume enclosed by the two separatrices, ∂V its boundary (the separatrices), $\vec{n}$ the local boundary normal, $\vec{v}$ the plasma velocity, and $\vec{v}_s$ the velocity of the separatrix surface itself. Note that the normal here is represented by the blue arrow in Figure 15.1 and must not be confused with the normal direction to the reconnecting current sheet.

Integrating the MHD energy equation over the volume V then leads to

$$\frac{d}{dt}\int_V dV\left[\rho\frac{v^2}{2}+\frac{B^2}{2\mu_o}+\frac{p}{\gamma-1}\right] = \oint_{\partial V} dS\,\vec{n}\cdot\left[-\frac{1}{\mu_o}\vec{R}\times\vec{B}+\frac{B^2}{\mu_o}\left(\frac{\vec{v}_s}{2}-\vec{v}\right)+\rho\frac{v^2}{2}\left(\vec{v}_s-\vec{v}\right)+\frac{p}{\gamma-1}\left(\vec{v}_s-\gamma\vec{v}\right)\right]. \quad (15.1)$$

AQ3

Here we have assumed the generic relation

$$\vec{E}+\vec{v}\times\vec{B}=\vec{R}, \quad (15.2)$$

where $\vec{R}\neq 0$ only inside the red-shaded region in Figure 15.1, implying that the first term on the right-hand side (RHS) of (1) can be ignored. Assuming a strictly two-dimensional system, we can represent the magnetic field through a flux function A such that

$$\vec{B}=\nabla A\times\vec{e}_y, \quad (15.3)$$

where $\vec{e}_y$ is the unit vector in the direction of the ignorable coordinate y. In the Coulomb gauge, the time evolution of the magnetic field can then be described by

$$\frac{\partial A}{\partial t}+\vec{v}\cdot\nabla A=-R_y. \quad (15.4)$$

At the X point proper, the gradient of A vanishes. At the same time, the numerical value A_x of the flux function at the X point is constant along the evolving separatrix surfaces, implying

$$\left.\frac{\partial A}{\partial t}\right|_{\text{separatrix}}=-R_y\big|_{X\text{ point}}. \quad (15.5)$$

Away from the diffusion region, the magnetic field is frozen into the plasma such that

$$\frac{\partial A}{\partial t}+\vec{v}\cdot\nabla A=0. \quad (15.6)$$

This is the change of A seen by a moving plasma element. If, at the separatrix, this change is the same as the one defined by (5), plasma does not cross the separatrix, and magnetic reconnection does not occur.

For reconnection, the surface and plasma velocities hence satisfy, on the separatrix,

$$\left(\vec{v}_s-\vec{v}\right)\cdot\nabla A\big|_{\text{separatrix}}=\left(\vec{v}_s-\vec{v}\right)\cdot\vec{n}B=-R_y\big|_{X\text{ point}}=-E_r. \quad (15.7)$$

AQ4

We can insert this result into the energy balance to yield

$$\frac{d}{dt}\int_V dV\left[\rho\frac{v^2}{2}+\frac{B^2}{2\mu_o}+\frac{p}{\gamma-1}\right] = \oint_{\partial V} dS\left[\left(\rho\frac{v^2}{2}+\frac{B^2}{2\mu_o}+\frac{p}{\gamma-1}\right)\frac{E_r}{B_{\text{separatrix}}}-\vec{n}\cdot\vec{v}_s\left(\frac{B^2}{2\mu_o}+p\right)\right]. \quad (15.8)$$

Equation (15.8) describes two contributions to the change of overall energy content of the volume enclosed by the separatrix: a compression or expansion contribution (second term on RHS) and a net energy transport facilitated by the reconnection electric field.

Similar arguments are readily made for mass and momentum transport. The analysis presented here shows that reconnection is a key transport mechanism, which, by opening otherwise closed magnetic surfaces, allows for significant changes to energy content. This feature is a critically important provider of energy sources for

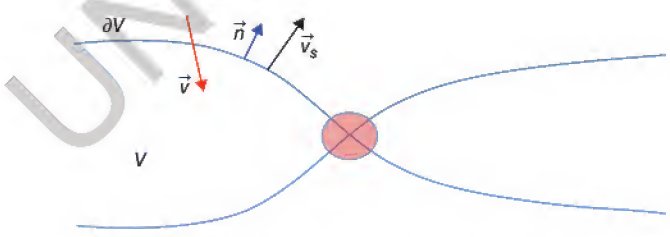

Figure 15.1 Schematic of the reconnection geometry.

the multitude of physical processes occurring inside the reconnected plasma.

In the following sections, we focus on the kinetic essentials, which render reconnection possible in collisionless plasmas. Arguably, the most important aspect here is the physics of the diffusion region, which supports the electric field that regulates the overall transport. We will present aspects of the collisionless physics of the diffusion region for two different environments: symmetric and asymmetric geometries.

15.3. TIME-DEPENDENT RECONNECTION

Time dependence and plasmoid formation have attracted considerable attention [e.g., *Daughton et al.*, 2006, 2009; *Drake et al.*, 2006; *Karimabadi et al.*, 2007]. We here perform a detailed analysis of the correlation between diffusion region dimensions and reconnection rate. For this purpose, we employ open boundary condition calculations of a continuously driven reconnecting system. The employed code is a 2.5D variant of our proven 3D particle-in-cell code [*Hesse et al.*, 1999], where periodic boundary conditions have been replaced by open boundaries, where normal derivatives of density, velocity, and isotropic pressure are assumed to vanish. AQ5 Here and in Chapter 16 we normalize densities by a typical density n_0 in the current sheet, the magnetic field by the asymptotic value B_0 of the in-plane magnetic field. Ions are assumed to be protons (mass m_p) throughout, and length scales by the ion inertial length c/ω_i, where the ion plasma frequency $\omega_i = \sqrt{e^2 n_0/\varepsilon_0 m_p}$ is evaluated for the reference density. Velocities are measured in units of the ion Alfvén velocity $v_A = B_0/\sqrt{\mu_0 m_p n_0}$ based on the reference magnitudes of magnetic field and density. The electric field is measured in units of $E_0 = v_A B_0$ and the pressure in units of $p_0 = B_0^2/\mu_0$. The above length scale and Ampere's law imply that the current density is normalized to $j_0 = \omega_i B_0/c\mu_0$.

The initial condition consists of a poloidal magnetic field, a modified Harris sheet [*Harris*, 1962] with a current AQ6 sheet half width of half the ion inertial length. The initial magnetic field is coplanar, i.e., does not contain a guide field component. In a coordinate system where the x axis is in the direction of the initial magnetic field, the y axis is in the initial current direction, and the z direction completes a right-handed coordinate system, it is of the following form:

$$B_x = \tanh(2z) + a_0 \pi/L_z \cos(2\pi x/L_x)\sin(\pi z/L_z), \quad (15.9a)$$

$$B_z = -a_0 2\pi/L_z \sin(2\pi x/L_x)\cos(\pi z/L_z). \quad (15.9b)$$

The perturbation amplitude $a_0 = 0.1$ leads to an initial value of the normal magnetic field of about 3% of B_0. The system size is $L_x = 100$ and $L_z = 25$. The ion-electron mass ratio is chosen to be $m_i/m_e = 25$. A total of 2×10^8 macroparticles are moved on a 1600×800 grid, with an electron/ion temperature ratio of $T_e/T_i = 0.2$. The system is, at its upper boundary, subjected to a constant driving electric field of $E_y = 0.185$. Particles are fed into the calculation to maintain, at the upper and lower boundaries, a density of $n_b = 0.2$ throughout the calculation and removed as they leave the boundaries at $x = 0$ and $x = 100$. The calculation extends for 1000 Alfvén times. Figure 15.2 displays two typical times of the simulation.

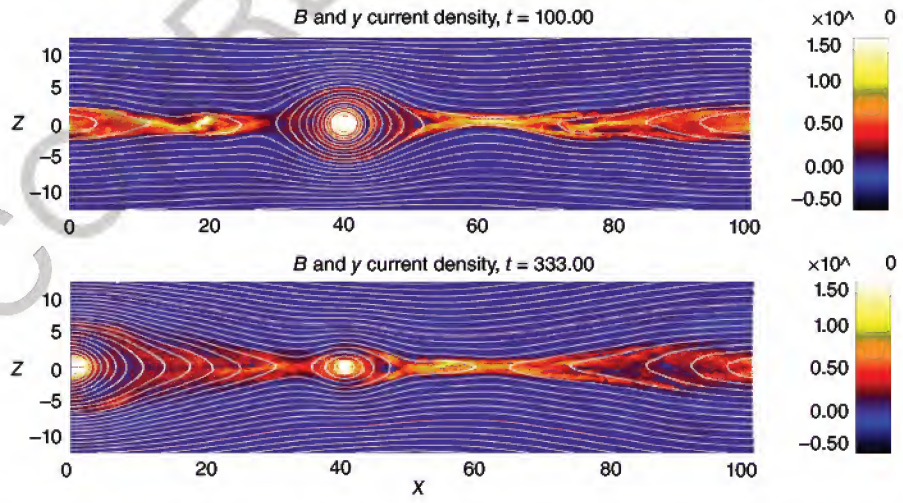

Figure 15.2 Two times of the simulation showing the common presence of magnetic islands at different times of the simulation. Note that the island shown in the bottom panel formed newly and did not evolve from the island shown in the top panel.

In order to assess the effect of island formation on magnetic reconnection, we need to define the dimensions of the diffusion region. The electric field is given by

$$\vec{E}+\vec{v}_e\times\vec{B}=-\frac{1}{en_e}\nabla\cdot\vec{P}_e-\frac{m_e}{e}\frac{d\vec{v}_e}{dt}=\vec{R}_e. \quad (15.10)$$

Here the index e denotes electron quantities. At each X point, the electric field is given entirely by the nonideal terms on the RHS of (10). When deviating either horizontally or vertically from the diffusion region location, the contribution to the electric field by the convective term (second term on the left-hand side (LHS)) begins to increase, whereas the nonideal contribution decreases. The horizontal and vertical edges of the diffusion region are now defined to be the location of crossover between ideal and nonideal terms, i.e.,

$$-\left(\vec{v}_e\times\vec{B}\right)\cdot\vec{e}_y=R_{ey}. \quad (15.11)$$

Equation 15.11 defines one location each to the right and left and top and bottom of the X point. The distance between the horizontal crossover points defines the length λ_x and the corresponding vertical distance λ_z is defined similarly. We perform this analysis for the dominant X point for each inverse ion cyclotron period during the simulation. The dominant X point is defined to be the one whose associated separatrix encloses the larges amount of magnetic flux.

We expect a dependence of the reconnection electric field on the ratio of the two quantities. This expectation is demonstrated in Figure 15.3, which plots the instantaneous electric field at the dominant X point against the diffusion region aspect ratio.

The figure shows a clear correlation of the expected kind. It is noteworthy, albeit not surprising, that the electric field values fluctuate about the applied electric field. The mean reconnection electric field strength equals the driving value; however, reconnection remains fast at all times. Applying a lower or larger driving electric field will likely lead to a smaller or larger, respectively, average reconnection rate and shift the distribution accordingly.

The point we want to make here is that the variation of the electric field is essentially due only to the variation of the diffusion region length in the x direction. For this purpose, Figure 15.4 illustrates the dependence of the electric field on the inverse diffusion region length in x, and Figure 15.5 depicts a histogram of encountered scale length in the z direction.

The clear correlation of the reconnection electric field with the inverse diffusion region length in the x direction combined with the very limited variation of the diffusion region thickness, implies the variation of the

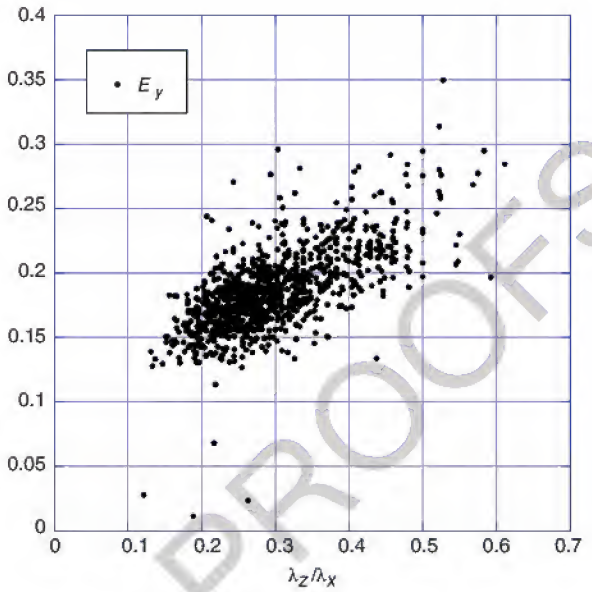

Figure 15.3 Scatter plot of the instantaneous electric field at the major X point against the aspect ratio of the diffusion region. The outliers in the reconnection rates are caused by unusually strongly fluctuating electric fields and plasma properties, which render an analysis very difficult.

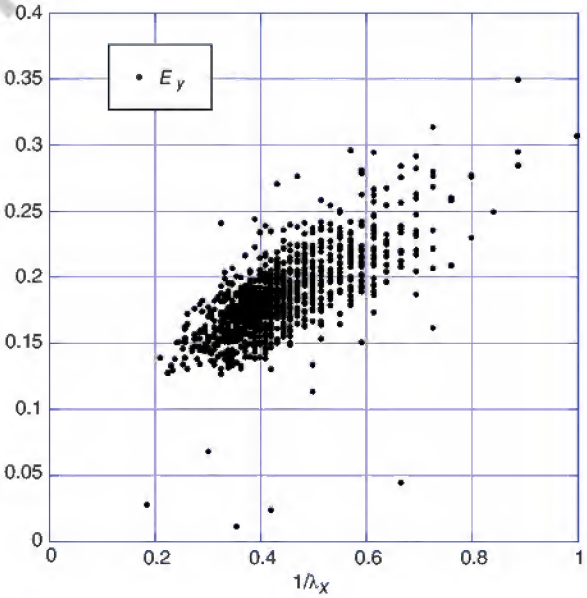

Figure 15.4 Variation of the reconnection electric field at the dominant X point with inverse diffusion region scale length in the x direction. The distribution of inverse diffusion region lengths has a mean of 0.54 and a standard deviation of 0.27.

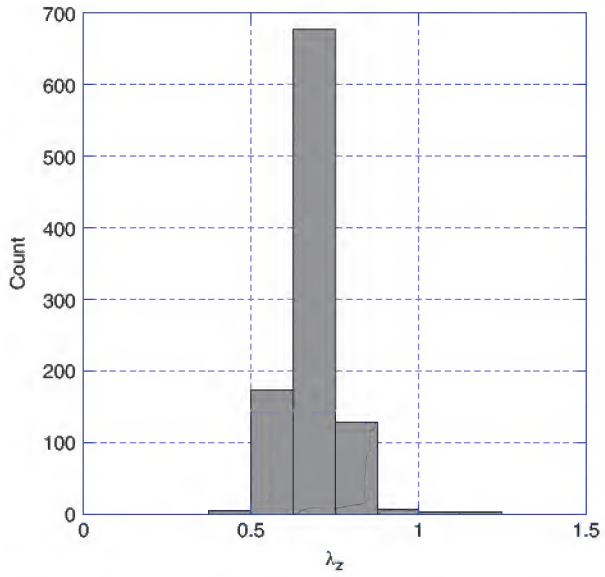

Figure 15.5 Histogram of diffusion region thicknesses throughout the calculation. The figure demonstrates only very small variations of this parameter. The distribution has a mean of 0.67 with a standard deviation of 0.09.

reconnection electric field is primarily due to variations of the diffusion region dimensions in the x direction. This latter variation is caused by changes to the electron magnetization in the horizontal direction, which extends or contracts the extent of the diffusion region. Electron magnetization is primarily affected by the strength of the magnetic field.

It appears evident that the growth of tearing mode islands, which form in the reconnecting current layer, are the prime cause of the variation of this magnetization. As a tearing mode island becomes nonlinear, it will begin to magnetize electrons and thus shorten the electron bounce width in the x direction. This leads to an effective shortening of λ_x, which, as we have seen above, will typically lead to a faster reconnection rate. Therefore, we conclude that island formation in the current layer associated with an active X point can increase the rate of magnetic reconnection. However, we note that reconnection can be fast for longer diffusion regions, presumably related to the absence of islands in the proximity of the X point under consideration. Figure 15.4 clearly shows that the rate virtually never drops below $E=0.12$. We point out that the applied electric field exceeds the empirical minimum values. Hence it is conceivable that plasmoid formation may be necessary to raise the average reconnection rate to that required for the flux transport prescribed by the external driving.

15.4. RECONNECTION LINE ORIENTATION FOR ASYMMETRIC RECONNECTION

In this section, we review recent results [*Hesse et al.*, 2013] pertaining to another aspect of magnetic reconnection: merging of plasmas from asymmetric inflow regions. Such asymmetry is commonly found at the magnetopause of Earth as well as on other planets. Typically, the shear angle of the magnetic field is different from the 180° modeled above, which, in comparison, is represented by the presence of a guide magnetic field. Here a key question is which direction a reconnection line will follow: Will it be normal to the plane wherein the guide field is constant [*Sonnerup*, 1974] or will it choose a different direction [*Gonzales and Mozer*, 1974; *Cowley*, 1976]? In order to address this question, we model a sample system with parameters set up similar to *Pritchett* [2008]. The poloidal magnetic field is of the form

$$B_x = 0.5 + tanh\left[z/l\right] \tag{15.12}$$

with a guide magnetic field

$$B_y = B_{y0} = 1. \tag{15.13}$$

The initial ion and electron densities are chosen to exhibit asymptotic values of $n=1$ for $z>0$ and $n=0.333$ for $z<0$:

$$n_i = n_e = 1 - tanh\left[z/l\right]/3. - tanh^2\left[z/l\right]/3. \tag{15.14}$$

The initial current layer half-width is $l=0.5$. A temperature of $T_e/T_i=0.2$ and a temperature of $T=T_i+T_e=1.5$ are employed. A small, X-type, initial perturbation is AQ5
introduced into current density and magnetic fields with an amplitude of $\delta B=0.1$, leading, e.g., to a form of B_z similar to (9b).

Particles, initialized as drifting Maxwellians, are integrated on a grid of 1000×800 cells representing a system of size $L_x=64$ and $L_z=25.6$. Periodic boundary conditions are employed in the x direction, whereas the particles are specularly reflected at the upper and lower boundaries. The ion-electron mass ratio is chosen to be $m_i/m_e=25$. A total of 1.6×10^9 macro particles are employed for the simulations.

In addition to investigating the reference case above, we further study the guide field model in coordinate systems of different orientation, derived from the one above by rotation around the z axis. The rotation angle α is defined in Figure 15.6. For each simulation in a rotated coordinate system, the entire set of vector quantities defined above is transformed into the rotated coordinate system, and the numerical model is applied to the new initial condition.

The overall evolution of the reference system, with uniform guide field of unity (i.e., $\alpha=0$), is illustrated for

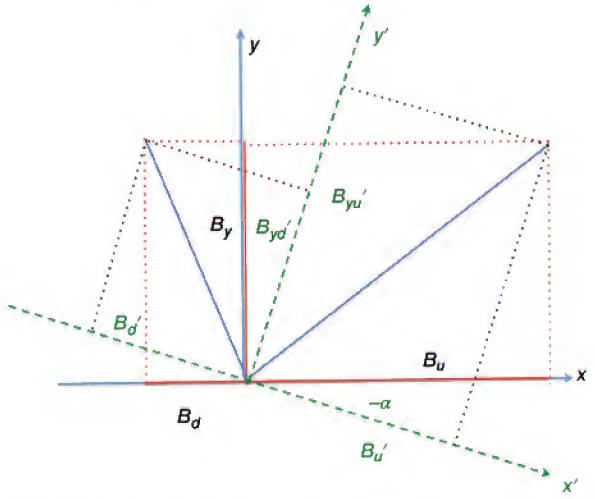

Figure 15.6 Graphics of the asymptotic magnetic field values in a coordinate system rotated by an angle α about the z axis. The indices u (up) and d (down) refer to asymptotic values above and below the current layer, respectively. The globally constant guide field $B_y = 1$ for $\alpha = 0$ becomes spatially dependent after rotation. The asymptotic values are shown on the y' axis.

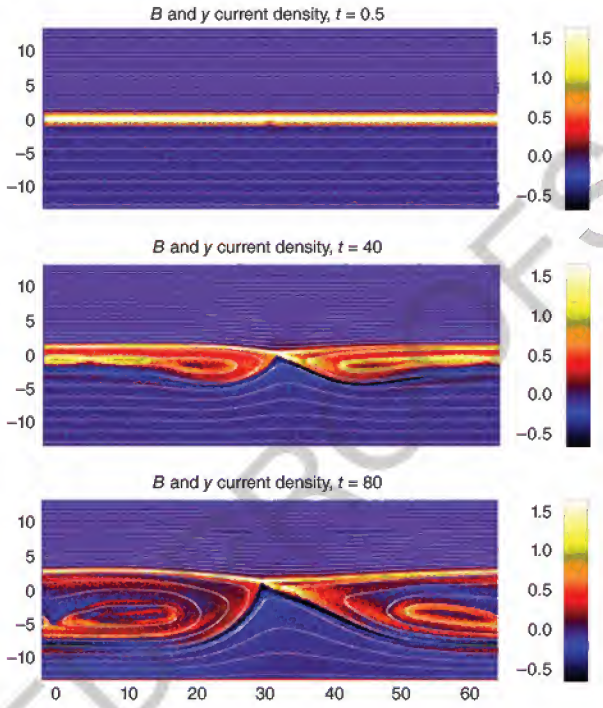

Figure 15.7 Magnetic field (white lines) and current density (color) evolution for the reference run, for which the initial guide field is uniform and of unit value.

three different times in Figure 15.7. The figure shows a transition from initially symmetric behavior to the development of a significant left-right asymmetry toward the end of the simulation period ($t = 80$).

The temporal evolution of the reference reconnection rate is shown in Figure 15.8. The figure demonstrates that *Sonnerup*'s [1974] prediction of fast reconnection in the presence of a guide field is correct: The peak reconnection rate is still about 0.05. The simulation never attains a steady state, a consequence of both periodic boundary conditions in the x direction and the closed top and bottom boundaries, which imply limited amount of magnetic flux and energy to tap into. Open boundary conditions for asymmetric systems are difficult to implement, which led us to choose the present implementation.

A reasonable assumption has the X line naturally orienting itself in such a way to obtain the fastest reconnection rate. The most important question is therefore whether faster reconnection can be obtained if $\alpha \neq 0$. Conducting a set of simulations, we find substantial variations of the reconnection rates depending on the orientation of the coordinate system. Figure 15.9 displays the time evolution of the reconnection rates for all runs obtained from the guide field reference model by coordinate system rotation and illustrates this strong dependence.

Figure 15.9 exhibits a maximum reconnection rate for $\alpha = -14.87°$. Adjacent values of the rotation angle yield almost identical reconnection rates, indicating that the maximum is not strongly localized. Extending rotation

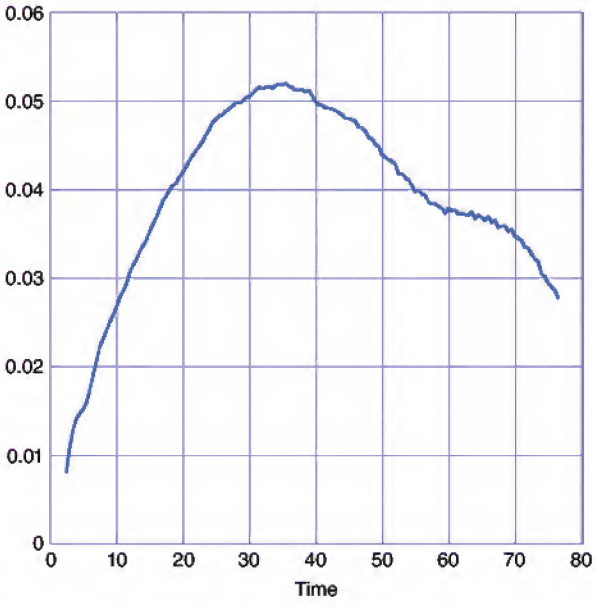

Figure 15.8 Time evolution of the reconnection electric field for the reference run for which the initial guide field is uniform and of unit value.

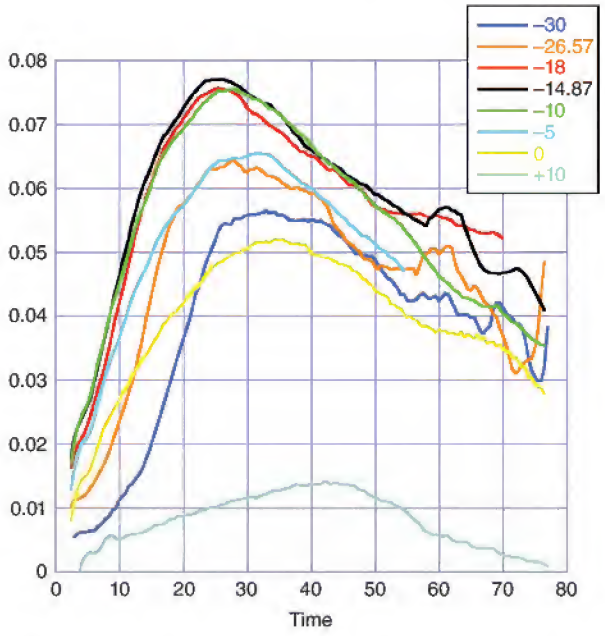

Figure 15.9 Time evolution of the reconnection electric field for the entire set of runs derived from rotating the frame of the guide field calculation by an angle α. The different colors denote different runs, and the angles are denoted in the figure.

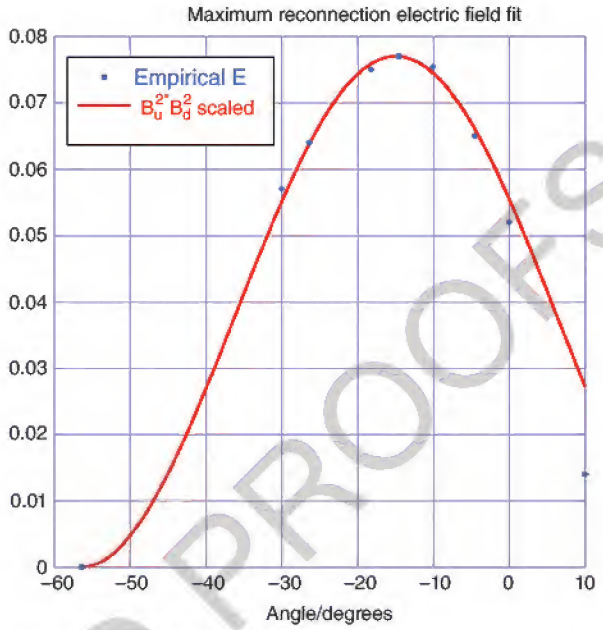

Figure 15.10 Plot of peak electric field values and predictions based on the magnetic energy available for magnetic reconnection. The magnetic-energy-based prediction exhibits an excellent match.

angles more significantly to either side, however, yields rapidly decreasing values of the reconnection electric fields. It is noteworthy that the reconnection evolution for $\alpha = -26.57°$, for which the reconnection magnetic fields are equal on both sides, still leads to considerably slower reconnection rates than the runs for smaller rotation angles. Therefore, symmetry of the in-plane magnetic field does not lead to the fastest reconnection rates.

Furthermore, the reconnection rate has to vanish for rotations, for which one of the two rotated magnetic field components

$$B_{u'} = B_u \cos(\alpha) + B_y \sin(\alpha), \tag{15.15}$$

$$B_{d'} = B_d \cos(\alpha) + B_y \sin(\alpha) \tag{15.16}$$

vanishes. For the system investigated here, $B_u = 1.5$ and $B_d = -0.5$. We find $B_u' = 0$ for the rotation value $\alpha \approx -57°$.

In order to develop a scaling relation for the reconnection electric field, we consider the maximum value of the entire time evolution for a fixed rotation angle. The key question is how the maximum values shown here relate to physical parameters. We will approach this issue from two different angles. First, we will make a reasonable assumption: reconnection rates should scale with the available magnetic energy. Because of the constancy of the total volume, this assumption implies that reconnection rates should be proportional to the magnetic energy density. Since the energy densities available for reconnection can differ across the current layer, our assumed proportionality implies

$$E_r = \psi_1 B_{u'}^2 B_{d'}^2, \tag{15.17}$$

where the factor ψ_1 should depend on parameters such as density and total magnetic field, which are held constant in the present investigation. Figure 15.10 demonstrates that the model (17) does an excellent job representing the maxima of the modeled reconnection rates.

We can use our model (17) to derive the rotation angle, for which this energy product assumes its maximum. Using the rotated magnetic field expressions (15) and (16), it is a straightforward exercise to derive the equation

$$\cot^2 \alpha_{max} - 2\frac{B_d B_u - B_y^2}{B_y (B_u + B_d)} \cot \alpha_{max} - 1 = 0 \tag{15.18}$$

for the angle α_{max}, for which (17) attains its maximum. The relevant solution is

$$\alpha_{max} = -14.87°,$$

matching our empirical determination.

It is further interesting to note that equation 15.18 also describes exactly the angle which bisects the angle between the asymptotic magnetic field on both sides of the current layer, a result readily derived from geometric considerations. This result applies to more than the system modeled here and is hence quite generic: The half-angle direction maximizes the magnetic energy available for reconnection.

In summary, our results indicate that the magnetic reconnection line in asymmetric systems is preferentially oriented in such a way that it bisects the direction of the asymptotic magnetic field direction on both inflow sides. This orientation is identical to the one for which the product of available magnetic energy is maximized.

15.5. SUMMARY

In this chapter, we presented results pertaining to three different aspects of magnetic reconnection. The first aspect, transport of magnetic flux, mass, momentum, and energy, is generic to all geometries and environments in which reconnection is operating. Focusing on energy transport, we could show that magnetic reconnection enables effective energy transport beyond what is possible by compression or expansion of a volume enclosed by a separatrix. We showed that the critical quantity providing the amplitude of the transport rate is exactly the reconnection electric field, measured at the X point. While not developed here, it is straightforward to develop similar analyses for mass and momentum transport.

Having demonstrated that effective energy transport is impossible without magnetic reconnection, we embarked on a discussion of the second topic: time dependence. Using our open boundary condition models, we executed an extended calculation of a driven, continuously reconnecting, symmetric current sheet.

For the purpose of the analysis of the model run, we defined diffusion region dimension through the region, where nonideal contributions to the electric field exceed the electric field contribution by electron convection. The magnitude crossover points were identified with the horizontal and vertical diffusion region edges. We developed an automated algorithm to calculate, for each output time step, these dimensions and take note of the instantaneous value of the reconnection electric field.

We then used the results for a statistical correlation. Not surprisingly, we found that rates tend to correlate well with the aspect ratio of the diffusion region. More surprisingly, we discovered that the aspect ratio variation was almost exclusively due to variation of diffusion region lengths, whereas diffusion region width showed relatively limited variations. We explained this phenomenon by the repetitive formation and growth of plasmoids, which, when grown past the linear stage, begin to magnetize electrons. This magnetization changes the crossover location between nonideal and convection electric fields and renders the diffusion region shorter. Thus, the aspect ratio becomes larger, and, on average, the reconnection electric field grows. This modulation is of the order of 50%, implying that reconnection is fast even in the temporary absence of magnetic islands. Therefore, our conclusion is that island formation is not necessary for fast reconnection, but it typically serves to enhance the reconnection rate substantially and in a very time-dependent manner.

As the third part of this chapter, we briefly reviewed recent results pertaining to the direction of the reconnection line in asymmetric magnetic reconnection. Starting with an asymmetric configuration with a guide magnetic field, which, in many ways, is typical for reconnection geometries expected at a planetary magnetopause, we performed a set of kinetic simulations of this system in rotated coordinate systems. We found a surprising variation in reconnection rates, even more surprising since neither constant guide field nor symmetric in-plane magnetic fields led to the fastest reconnection rate. Instead, we found empirically that the reconnection rates scaled well with the product of energy densities of both inflow regions. The direction which maximizes this product turned out to be also halving the angle between the asymptotic magnetic field directions on both sides of the current layer. Clearly, this result requires further testing, including for different density asymmetries but it is highly suggestive that the X line will orient itself such that it bisects the directions on the magnetic fields in the two inflow regions.

Finally, one might ask the question of how these results pertain to the magnetospheres of planets other than Earth. The general results presented in section 15.2. are universal, i.e., they apply, at least in principle, also to planetary magnetospheres. As the analysis in subsequent sections has been conducted in dimensionless units, a large variety of applications can be developed by employing appropriate dimensions in the interpretation of the results. This freedom is an application of the "Vlasov scaling" [*Schindler*, 1969], whereby Vlasov scaling laws permit rescaling of solution to different applications. Such rescaling will greatly extend the applicability of the results presented here; however, just as in the terrestrial magnetosphere, rescaling will fall short of covering all relevant scenarios. Therefore, much more research needs to be conducted, and many more exciting and surprising discoveries lie in wait.

Acknowledgments. This work was supported by NASA's Magnetospheric MultiScale Mission. One of us (N.A.) gratefully acknowledges support from the NASA Postdoctoral fellowship program.

REFERENCES

Antiochos, S. K., C. R. DeVore, and J. A. Klimchuk (1999), A model for solar coronal mass ejections, *Astrophys. J.*, *510*, 485–493.

Aunai, N., G. Belmont, and R. Smets (2011), Energy budgets in collisionless magnetic reconnection: Ion heating and bulk acceleration, *Phys. Plasmas*, *18*, 2901.

Birn, J., J. F. Drake, M. A. Shay, B. N. Rogers, R. E. Denton, M. Hesse, M. Kuznetsova, Z. W. Ma, A. Bhattacharjee, A. and Otto, and P. L. Pritchett (2001), GEM magnetic reconnection challenge, *J. Geophys. Res.*, *106*, 3715.

Birn, J., M. Hesse, and S. Zenitani, (2011), Reconnection in compressible plasmas: Extended conversion region, *Phys. Plasmas*, *18*, 111,202.

Cassak, P. A., and M. A. Shay (2007), Scaling of asymmetric magnetic reconnection: General theory and collisional simulations, *Phys. Plasmas*, *14*, 102,114.

Cowley, S. W. (1976), Comments on the merging of nonantiparallel magnetic fields, *J. Geophys. Res.*, *81*, 3455.

Drake, J. F., M. Swisdak, K. M. Schoeffler, B. N. Rogers, and S. Kobayashi (2006), Formation of secondary islands during magnetic reconnection, *Geophys. Res. Lett.*, *33*(13), L13105, doi:10.1029/2006GL025957.

Daughton, W., J. Scudder, and H. Karimabadi, (2006), Fully kinetic simulations of undriven magnetic reconnection with open boundary conditions, *Phys. Plasmas*, *13*, 2101.

Daughton, W, V. Roytershteyn, B. Albright, H. Karimabadi, L. Yin, and K. J. Bowers (2009), Transition from collisional to kinetic regimes in large-scale reconnection layers, *Phys. Rev. Lett.*, *103*, 65,004.

Eastwood, J. P., T.-D. Phan, F. S. Mozer, M. A. Shay, M. Fujimoto, A. Retinò, M. Hesse, A. Balogh, E. A. Lucek, and I. Dandouras (2007), Multi-point observations of the Hall electromagnetic field and secondary island formation during magnetic reconnection, *J. Geophys. Res.*, *112*, A06235, doi:10.1029/2006JA012158.

Eastwood, J., T. Phan, M. Øieroset, and M. Shay (2010), Average properties of the magnetic reconnection ion diffusion region in the Earth's magnetotail: The 2001–2005 Cluster observations and comparison with simulations, *J. Geophys. Res.*, *115*, 08215.

Gonzales, W. D., and F. S. Mozer (1974), A quantitative model for the potential resulting from reconnection with an arbitrary interplanetary magnetic field, *J. Geophys. Res.*, *79*, 4186.

Gosling, J. T., J. Birn, and M. Hesse (1995), Three-dimensional magnetic reconnection and the magnetic topology of coronal mass ejection events, *Geophys. Res. Lett.*, *22*, 869.

Gosling, J. T., R. M. Skoug, D. J. McComas, and C. W Smith (2005), Direct evidence for magnetic reconnection in the solar wind near 1 AU, *J. Geophys. Res.*, *110*, 2156.

Hesse, M., J. Birn, D. N. Baker, and J. A. Slavin (1996), MHD simulations of the transition of magnetic reconnection from closed to open field lines, *J. Geophys. Res.*, *101*, 10,805.

Hesse, M., K. Schindler, J. Birn, and M. Kuznetsova (1999), The diffusion region in collisionless magnetic reconnection, *Phys. Plasmas*, *6*, 1781.

Hesse, M., J. Birn, and S. Zenitani (2011a), Magnetic reconnection in a compressible MHD plasma, *Phys. Plasmas*, *18*, 042,104. AQ7

Hesse, M., T. Neukirch; K. Schindler, M. Kuznetsova, and S. Zenitani (2011b), The diffusion region in collisionless magnetic reconnection, *Space Sci. Rev.*, *160* (1–4) 3.

Hesse, M., N. Aunai, S. Zenitani, M. Kuznetsova, and J. Birn (2013), Aspects of collisionless magnetic reconnection in asymmetric systems, *Phys. Plasmas*, *20*, 1210.

Hones, E. W., Jr. (1977), Substorm processes in the magnetotail: Comments on "On hot tenuous plasma fireballs and boundary layers in the earth's magnetotail" by L. A. Frank, K. L. Ackerson, and R. P. Lepping, *J. Geophys. Res.*, *82*, 5633.

Huang, Y.-M., and A. Bhattacharjee (2013), Plasmoid instability in high-Lundquist-number magnetic reconnection, *Phys. Plasmas*, *20*, 055,702.

H. Karimabadi, W. Daughton, and J. D. Scudder (2007), Multi-scale structure of the electron diffusion region, *Geophys. Res. Lett.*, L13104, doi:10.1029/2007GL030306.

Mozer, F., V. Angelopoulos, J. Bonnell, K.-H. Glassmeier, and J. McFadden (2008), THEMIS observations of modified Hall fields in asymmetric magnetic field reconnection, *Geophys. Res. Lett.*, *35*. AQ8

Mozer, F. S., and P. L. Pritchett (2011), Electron physics of asymmetric magnetic field reconnection, *Space Sci. Rev.*, *158*, 119.

Paschmann, G. (2008), Recent in-situ observations of magnetic reconnection in near-Earth space, *Geophys. Res. Lett.*, *35*, 19,109.

Pritchett, P. L. (2008), Collisionless magnetic reconnection in an asymmetric current sheet, *J. Geophys. Res.*, *113*, A06210, doi:10.1029/2007JA012930.

Schindler, K. (1969), Laboratory experiments related to the solar wind and the magnetosphere, *Rev. Geophys.*, *7*, 51.

Sonnerup, B. U. O. (1974), Magnetopause reconnection rate, *J. Geophys. Res.*, *79*, 1546.

Swisdak, M., B. N. Rogers, J. F. Drake, and M. A. Shay (2003), Diamagnetic suppression of component magnetic reconnection at the magnetopause, *J. Geophys. Res.*, *108*, doi:10.1029/2002JA009726.